

The B Anomalies, the U_1 Leptoquark and Dark Matter

Geneviève Bélanger ^{a,1}, Jacky Kumar ^{b,c,2}, David London ^{b,3} and Alexander Pukhov ^{d,4}

a: LAPTh, CNRS, USMB, 9 Chemin de Bellevue, 74940 Annecy, France

b: Physique des Particules, Université de Montréal,

1375 Avenue Thérèse-Lavoie-Roux, Montréal, QC, Canada H2V 0B3

c: Institute for Advanced Study, Technical University Munich,

Lichtenbergstr. 2a, D-85747 Garching, Germany

d: Skobeltsyn Institute of Nuclear Physics,

Moscow State University, Moscow 119992, Russia

(June 24, 2022)

Abstract

The present-day B -anomalies involving $b \rightarrow s\mu^+\mu^-$ or $b \rightarrow c\tau^-\bar{\nu}$ transitions can all be explained with the addition of a vector U_1 leptoquark with a mass of $M_{U_1} \gtrsim 1.8$ TeV. In the scalar singlet dark matter model (SSDMM), the DM is a scalar S that couples to the Higgs via $\lambda_{hS} S^2 |H|^2$. We update the fit to the data and find that the SSDMM is now viable only for $M_S \gtrsim 1.6$ TeV. In this paper, we assume that the DM also couples to the U_1 via $\lambda_{U_1 S} S^2 U_{1\mu}^\dagger U_1^\mu$. In addition to leading to DM annihilation via $SS \rightarrow U_1 \bar{U}_1$, this coupling generates $SSgg$ and $SS\gamma\gamma$ couplings at one loop. Although naively divergent, these loop diagrams can be calculated under the assumption that the U_1 is a gauge boson of a group broken at the TeV scale. With this DM- U_1 coupling term, there are additional contributions to the various DM observables (relic density, direct and indirect detection). We find that the constraints on the SSDMM are relaxed for both heavy DM ($M_S \gtrsim M_{U_1}$) and light DM ($M_S < M_{U_1}$).

¹belanger@lapth.cnrs.fr

²jacky.kumar@tum.de

³london@lps.umontreal.ca

⁴alexander.pukhov@gmail.com

1 Introduction

At the present time, there are discrepancies with the predictions of the standard model (SM) in measurements of a variety of observables in B decays (for a review, see Ref. [1]). First, there are observables involving the neutral-current transition $b \rightarrow s\mu^+\mu^-$. These include the branching ratios and angular distributions of $B \rightarrow K^*\mu^+\mu^-$ and $B_s \rightarrow \phi\mu^+\mu^-$, $\mathcal{B}(B_s \rightarrow \mu^+\mu^-)$, and the lepton-flavour-universality-violating (LFUV) ratios $R_{K^{(*)}} \equiv \mathcal{B}(\bar{B} \rightarrow K^{(*)}\mu^+\mu^-)/\mathcal{B}(\bar{B} \rightarrow K^{(*)}e^+e^-)$. When all the data are combined in a global fit with close to 250 $b \rightarrow s\mu^+\mu^-$ observables [2], it is found that the overall disagreement with the SM is at the level of 2.5σ . A variety of new-physics (NP) models have been proposed to explain this, the simplest involving the addition of a Z' boson or a (scalar or vector) leptoquark (LQ) [1].

There are also anomalies in observables involving the charged-current decay $b \rightarrow c\tau^-\bar{\nu}$ [1], in particular the LFUV ratios $R_{D^{(*)}} \equiv \mathcal{B}(\bar{B} \rightarrow D^{(*)}\tau^-\bar{\nu}_\tau)/\mathcal{B}(\bar{B} \rightarrow D^{(*)}\ell^-\bar{\nu}_\ell)$ ($\ell = e, \mu$) and $R_{J/\psi} \equiv \mathcal{B}(B_c^+ \rightarrow J/\psi\tau^+\nu_\tau)/\mathcal{B}(B_c^+ \rightarrow J/\psi\mu^+\nu_\mu)$. Here the discrepancy is somewhat larger, at the level of $\sim 3.3\sigma$ [3]. Once again, various NP explanations have been proposed, with most involving a W' boson, a LQ, or a charged Higgs boson [1].

In Ref. [4], it was pointed out that it is possible to construct a NP model that explains both kinds of B anomalies. In such a model, the NP contributions to neutral-current and charged-current processes would have to be related, which can occur if the NP couplings are left-handed. Possible NP particles include a vector-boson triplet (W', Z'), as well as several different types of LQs.

These models were analyzed in Refs. [5–7]. Although they can in principle explain the B anomalies, all of these models also contribute to other processes, whose measurements place constraints on the models. These include B_S^0 - \bar{B}_S^0 mixing, $b \rightarrow s\bar{\nu}\nu$ and $\tau \rightarrow \mu\phi$ decays, etc. When all such constraints are taken into account, as well as those from direct searches at the LHC, only one model survives. It uses a vector $SU(2)_L$ -singlet leptoquark (LQ) of charge $-2/3$, known as U_1 . Thus, all B anomalies can be explained with the addition of the U_1 LQ⁵.

Another observation that requires physics beyond the SM is dark matter (DM). Although DM is the most prevalent form of matter in the universe, we know very little about its nature. It must be neutral (or very nearly so), but we have no knowledge about its mass or spin. It was present in the early universe, so its presence today indicates that it must be stable. This is most likely due to a symmetry, usually taken to be Z_2 , under which the DM and SM particles have opposite charges. The relic density of DM is determined precisely from the observations of the Cosmic Microwave Background [9]. In the standard freeze-out mechanism, the rate of DM

⁵Another (somewhat less-elegant) possibility is to add the two scalar LQs S_1 and S_3 [8]. The $SU(2)_L$ -triplet S_3 contributes to both $b \rightarrow s\mu^+\mu^-$ and $b \rightarrow c\tau^-\bar{\nu}$, while the $SU(2)_L$ -singlet S_1 contributes only to $b \rightarrow s\mu^+\mu^-$. By carefully choosing the couplings of S_1 and S_3 , both anomalies can be explained, while evading the constraints from $b \rightarrow s\nu\bar{\nu}$.

annihilation into SM particles determines the DM relic density. For these annihilations to take place, there must be a mediator that couples to the DM and to some SM particles. The exchange of this mediator will also produce DM elastic scattering on nuclei, allowing for the direct detection of DM, and DM annihilation in the galaxy, leading to indirect detection of DM in cosmic rays.

One of the simplest mediator scenarios is the scalar singlet dark matter model (SSDMM) [10–12]. Here the DM is assumed to be a scalar that couples to the SM Higgs boson through an $S^2|H|^2$ term. This Higgs portal leads to DM annihilation in the early universe via $SS \rightarrow h \rightarrow$ SM particles and to the scattering with nucleons, $SN \rightarrow SN$, via Higgs exchange, which contributes to direct detection. A global fit of the SSDMM was performed in 2017 [13], and it was found that the various constraints, particularly the DM relic density and the upper limit on direct detection, have the effect that the SSDMM is strongly disfavoured for $M_S \lesssim 500\text{--}700$ GeV.

Because the B anomalies and DM both offer strong hints of NP, it is quite natural to consider links between them. Indeed, a number of papers have proposed models in which the Z' used to explain the $b \rightarrow s\mu^+\mu^-$ anomalies also acts as the mediator for DM annihilation [14–26]. And a few papers have combined DM with LQs [27–31]. In one of these, the two scalar LQs S_1 and S_3 provide a portal for the scalar DM particle S via an $S^2|S_{LQ}|^2$ coupling ($S_{LQ} = S_1, S_3$) [30].

In the present paper, we apply this LQ portal idea to the U_1 LQ. For scalar DM S , we assume a coupling of the form $S^2 U_{1\mu}^\dagger U_1^\mu$. Such a coupling produces the tree-level annihilation process $SS \rightarrow U_1 \bar{U}_1$, which contributes to the relic density. At one loop, one can also generate an effective $SSgg$ coupling. This leads to $SS \rightarrow gg$ annihilation (relic density) and contributes to $SN \rightarrow SN$ (direct detection). The problem is that, because the U_1 LQ is a vector boson, such loop diagrams generally diverge. Fortunately, there is a way around this. The U_1 is generally considered to be a gauge boson of an extended gauge group that is broken at the TeV scale. In this case, the $SSgg$ coupling can be computed by analogy to the SM hgg or $h\gamma\gamma$ couplings. An $SS\gamma\gamma$ coupling, which contributes to indirect detection signals, is also induced, and can be calculated similarly.

In this paper, we examine the consequences of an $S^2 U_{1\mu}^\dagger U_1^\mu$ coupling for the various DM observables – relic density, direct detection and indirect detection – for different DM masses. We treat separately the cases of heavy DM ($M_S \gtrsim M_{U_1} = 1.8$ TeV), for which the annihilation process $SS \rightarrow U_1 \bar{U}_1$ is possible, and light DM ($M_S < M_{U_1} = 1.8$ TeV), for which it is not. In particular, we investigate whether the addition of the U_1 LQ can improve the prospects for the SSDMM. As we will see, it does do this, for both heavy and light DM.

In Sec. 2, we present the setup. We introduce the effective Hamiltonian that contains both U_1 and S , compute the one-loop coupling term $C_5^g S^2 G_{\mu\nu}^a G^{a\mu\nu}$ that yields an effective $SSgg$ coupling, and describe in more detail the SSDMM. The effects on the DM observables are examined in Sec. 3, with heavy and light DM studied separately. In the study of light DM, we also update the constraints on

the SSDMM. We find that, in both cases, the addition of the U_1 LQ can indeed make the constraints on the SSDMM less stringent, thus improving its outlook. We analyze the prospects for probing this model via DM indirect detection in the photon channels with the future Cherenkov Telescope Array detector. We conclude in Sec. 4.

2 Setup

The U_1 LQ is a vector boson. If one simply adds it to the SM, but makes no additions to the Higgs sector, the new theory is not renormalizable. As a consequence, loop diagrams with internal U_1 LQs, which can lead to potentially important effects, are generally divergent (some exceptions can be found in Ref. [32]). To deal with this problem, models have been constructed with an extended gauge group that contains the U_1 LQ as a gauge boson and is broken at the TeV scale. There are two types of such UV-completion models: (i) those based on variations of Pati-Salam models, in which $SU(4)_{PS}$ unifies $SU(3)_C$ and a $U(1)$ under which both quarks and leptons are charged [33–44], and (ii) those that use the “4321” gauge group, $SU(4) \times SU(3)' \times SU(2)_L \times U(1)_X$ [28, 45, 46]. In our analysis, we assume that the U_1 LQ is a gauge boson of a larger group, but make no assumptions about the group structure.

2.1 Effective Hamiltonian

We take Λ_{NP} to be the scale at which this larger gauge group is broken. Below Λ_{NP} , but above the electroweak-breaking scale, the U_1 and S are added to the particle spectrum. At leading order, the effective Lagrangian includes all operators up to mass dimension four that respect the $SU(3)_C \times SU(2)_L \times U(1)_Y$ SM gauge symmetry. The full Lagrangian is

$$\mathcal{L} = \mathcal{L}_{SM} + \mathcal{L}_S + \mathcal{L}_{U_1} + \mathcal{L}_Y + \mathcal{L}_{SU_1H} , \quad (1)$$

where

$$\mathcal{L}_S = \frac{1}{2} \partial_\mu S \partial^\mu S - \frac{1}{2} \mu_S^2 S^2 - \frac{1}{4} \lambda_S S^4 , \quad (2)$$

$$\begin{aligned} \mathcal{L}_{U_1} = & -\frac{1}{2} (D_\mu U_{1\nu} - D_\nu U_{1\mu})^\dagger (D^\mu U_1^\nu - D^\nu U_1^\mu) - M_{U_1}^2 U_{1\mu}^\dagger U_1^\mu \\ & - ig_{U_1 U_1 g} U_1^{\dagger\mu} T^a U_1^\nu G_{\mu\nu}^a - ig_{U_1 U_1 B} \frac{2}{3} U_1^{\dagger\mu} U_1^\nu B_{\mu\nu} , \end{aligned} \quad (3)$$

$$\mathcal{L}_Y = (g_L^{ij} \bar{Q}_i \gamma_\mu P_L L_j + g_R^{ij} \bar{d}_i \gamma_\mu P_R e_j) U_1^\mu + h.c. , \quad (4)$$

$$\mathcal{L}_{SU_1H} = -\frac{1}{2} \lambda_{U_1 S} S^2 U_{1\mu}^\dagger U_1^\mu - \frac{1}{4} \lambda_{hS} S^2 |H|^2 - \frac{1}{2} \lambda_{U_1 h} U_{1\mu}^\dagger U_1^\mu |H|^2 . \quad (5)$$

In \mathcal{L}_Y , i and j are generation indices, and

$$Q_L = \begin{pmatrix} V^\dagger u_L \\ d_L \end{pmatrix}, \quad L_L = \begin{pmatrix} \nu_L \\ e_L \end{pmatrix}, \quad (6)$$

where V is the Cabibbo-Kobayashi-Maskawa (CKM) matrix.

The U_1 portal term $S^2 U_{1\mu}^\dagger U_1^\mu$ contributes at tree level to the relic density via $SS \rightarrow U_1 \bar{U}_1$. This process is suppressed when the U_1 cannot be produced on-shell, so that the cross section depends strongly on the mass of the U_1 . In Ref. [47], using the latest LHC data and assuming that the LQ couples mainly to the third generation, it was determined that direct searches at the LHC place a lower limit of $M_{U_1} = 1.8$ TeV; this is the value we use in our analysis.

2.2 One-loop DM couplings

Direct detection experiments search for the elastic scattering process $SN \rightarrow SN$. This can be produced using the U_1 portal, but only at the one-loop level. For example, in Ref. [48], it is pointed out that, in some models, a coupling of SS to two gluons can be generated, and that this can mediate the $SN \rightarrow SN$ scattering process. Since the U_1 LQ is coloured, an $SSgg$ coupling can be generated at one loop through the diagrams in Fig. 1.

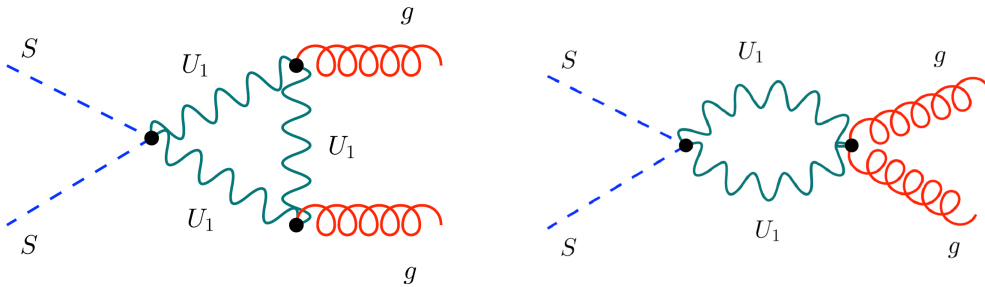


Figure 1: Diagrams generating the $SSgg$ coupling.

However, this is problematic: calculations of these diagrams can only be done in unitary gauge, and here there are serious divergences. Fortunately, in this case there is a solution.

First, consider the coupling of two U_1 LQs to the hypercharge boson B_μ . From Eq. (3), this is

$$\begin{aligned} \mathcal{L}_{U_1 U_1 B} = & ig' \frac{2}{3} \left[(\partial_\mu U_{1\nu}^\dagger - \partial_\nu U_{1\mu}^\dagger) B^\mu U_1^\nu - (\partial_\mu U_{1\nu} - \partial_\nu U_{1\mu}) B^\mu U_1^{\dagger\nu} \right. \\ & \left. + \frac{g_{U_1 U_1 B}}{g'} (U_{1\mu} U_{1\nu}^\dagger - U_{1\nu} U_{1\mu}^\dagger) \partial^\mu B^\nu \right]. \quad (7) \end{aligned}$$

From the point of view of the effective Lagrangian below Λ_{NP} , $g_{U_1 U_1 B}$ is an arbitrary constant. However, one must remember that both U_1 and B_μ are gauge bosons of the (unspecified) larger gauge group. As such, their interactions arise only from the gauge-boson kinetic term $F_{\mu\nu}^i F^{i\mu\nu}$ of this gauge group. This will necessarily generate the three terms above with equal weighting, i.e., $g_{U_1 U_1 B} = g'$, as occurs in the SM with the $W^+ W^- \gamma$ coupling terms. (See Ref. [49] for similar arguments in the context of $(g-2)_\mu$.) The coupling of two U_1 LQs to gluons can be treated similarly, leading to $g_{U_1 U_1 g} = g_s$.

Second, note that the diagrams in Fig. 1 are essentially the same as those of the SM process $h \rightarrow \gamma\gamma$ with internal W bosons, with the obvious changes of h replaced by SS , W by U_1 , and γ by g . As discussed above, the $U_1 \bar{U}_1 g$ and $U_1 \bar{U}_1 gg$ couplings have the same structure as the SM $W^+ W^- \gamma$ and $W^+ W^- \gamma\gamma$ couplings. In Ref. [50], the SM $h \rightarrow \gamma\gamma$ diagrams with internal W s are calculated in unitary gauge, and it is explicitly shown that the result is finite and gauge-independent.

A more general calculation can be found in Ref. [51]. There it is found that, for the effective coupling term $\lambda h F_{\mu\nu} F^{\mu\nu}$, the contribution to λ from $g_{hVV} M_V h V_\mu V^\mu$ is given by

$$\lambda = -\frac{\alpha}{8\pi} \frac{g_{hVV} f_V^c q_V^2}{2M_V} A(\tau) \quad , \quad \tau = \frac{M_h^2}{4M_V^2} . \quad (8)$$

Here q_V and f_V^c are the electric charge and the colour factor of the vector particle running in the loop. (For the W , $q_V = f_V^c = 1$.) The loop function is given by

$$A(x) = -\frac{1}{x^2} [2x^2 + 3x + 3(2x-1)f(x)] ,$$

$$\text{with } f(x) = \begin{cases} \arcsin^2(\sqrt{x}) & \text{for } x \leq 1 , \\ -\frac{1}{4} \left[\ln \frac{1+\sqrt{1-x^{-1}}}{1-\sqrt{1-x^{-1}}} - i\pi \right]^2 & \text{for } x > 1 . \end{cases} \quad (9)$$

In the limit of $x \rightarrow 0$, $A(x) \rightarrow -7$ [52].

From this we can deduce the coefficient of the effective coupling term $\alpha_s C_5^g S^2 G_{\mu\nu}^a G^{a\mu\nu}$ generated by the coupling $-\frac{1}{2} \lambda_{U_1 S} S^2 U_{1\mu}^\dagger U_1^\mu$. We make the substitutions $\alpha \rightarrow \alpha_s$, $g_{hVV} \rightarrow \frac{1}{2} \lambda_{U_1 S}$ and $f_V^c = \text{Tr}(T^a T^a) = \frac{1}{2}$ (q_V is not relevant). Also, in Eq. (8), $M_h^2 \rightarrow 2k_1 \cdot k_2$, where the k_i are the four-momenta of the gluons. Thus, this factor is process-dependent. We then have

$$C_5^g = -\frac{\lambda_{U_1 S}}{64\pi M_{U_1}^2} A(\tau) \quad , \quad \tau = \frac{k_1 \cdot k_2}{2M_{U_1}^2} . \quad (10)$$

The scattering process $SN \rightarrow SN$ takes place at energies of $O(\text{keV})$, so it is reasonable to consider the limit $\tau \rightarrow 0$. For DM annihilation in the early universe via $SS \rightarrow gg$, we have $k_1 \cdot k_2 \simeq 2M_S^2$.

The gluons in Fig. 1 can be replaced by photons, leading to an $SS\gamma\gamma$ coupling. Writing the effective coupling term as $\alpha C_5^\gamma S^2 F_{\mu\nu} F^{\mu\nu}$, and using $q_{U_1} = \frac{2}{3}$ and $f_{U_1}^c = 3$,

we have from Eq. (8) that

$$C_5^\gamma = -\frac{\lambda_{U_1 S}}{48\pi M_{U_1}^2} A(\tau) \quad , \quad \tau = \frac{k_1 \cdot k_2}{M_{U_1}^2} . \quad (11)$$

The $SS \rightarrow \gamma\gamma$ annihilation channel can be important for indirect detection, as we will discuss in Sec. 3.

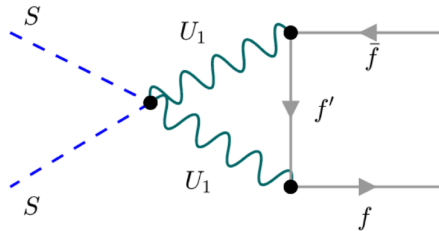


Figure 2: Diagram generating the $SS\bar{f}f$ coupling. If f is a quark, f' is a lepton and vice-versa.

Finally, another coupling that can be generated at one loop is $SS\bar{f}f$, where f is any SM fermion, see Fig. 2. However, in unitary gauge, this diagram diverges, so this coupling cannot be computed in the absence of a complete model. Even so, as we see below, a simple dimensional analysis is sufficient.

First, we note that it is usually assumed that the U_1 couples only to third-generation fermions in the gauge basis. The (smaller) couplings involving the second generation are generated when one transforms to the mass basis. In Ref. [7], it was shown that the B anomalies can be explained if the couplings are purely left-handed with

$$g_L^{33} = 1 \quad , \quad g_L^{23} = g_L^{32} = 0.28 \quad , \quad g_L^{22} = -0.008 \quad , \quad (12)$$

where the g_L^{ij} are the Yukawa couplings of Eq. (4), with $g_R^{ij} = 0$. The $SS\bar{f}f$ coupling then takes the form

$$SS\bar{f}f \sim \frac{\lambda_{U_1 S} |g_L^{ij}|^2}{16\pi^2 M_{U_1}^2} \left[m_f SS\bar{f}P_L f + S \overset{\leftrightarrow}{\partial}_\mu S \bar{f} \gamma^\mu P_L f \right] \quad , \quad (13)$$

where the fermion f can be a quark q_i or a lepton l_j .

We can use this to estimate the contribution to the relic density from the $SS\bar{f}f$ operator. The coefficients of the first and second terms are $O(10^{-7}) \text{ GeV}^{-1}$ (for $f = t$) and $O(10^{-9}) \text{ GeV}^{-2}$, respectively. Both of these $SS\bar{f}f$ couplings are examined in Ref. [53], and as can be seen from Fig. 5 of this paper, these coefficients are far too small to generate an important contribution to the relic density.

If f is a quark, the $SS\bar{f}f$ coupling could in principle contribute to $SN \rightarrow SN$ (direct detection). However, we see that this contribution is small: the Yukawa couplings are large only for third-generation quarks, whose presence in nucleons is

suppressed. Conversely, first-generation quarks are plentiful in nucleons, but the Yukawa couplings are tiny. The bottom line is that this contribution to $SN \rightarrow SN$ is negligible compared to that of $SSgg$.

2.3 Scalar Singlet Dark Matter Model

The scalar DM couples to the Higgs via the Higgs portal term in Eq. (5), $S^2|H|^2$. This coupling is the basis for the SSDMM [10–12].

After electroweak symmetry breaking, $H \rightarrow (h + v_0)/\sqrt{2}$, where h is the physical Higgs boson and $v_0 = 246$ GeV is the VEV of the Higgs field. Three terms are generated from the Higgs portal term:

$$-\frac{1}{4}\lambda_{hS}v_0^2S^2 - \frac{1}{2}\lambda_{hS}v_0S^2h - \frac{1}{4}\lambda_{hS}S^2h^2. \quad (14)$$

The terms v_0S^2h and S^2h^2 lead to DM annihilation via the processes $SS \rightarrow h \rightarrow W^+W^-, Z^0Z^0, hh, t\bar{t}, b\bar{b}, gg$, etc., and $SS \rightarrow hh$, respectively. Given the relic density of DM, and assuming that the S particles were in thermal equilibrium with ordinary matter throughout the evolution of the universe, the present-day value of the density of DM [9] fixes the value of λ_{hS} .

The v_0hS^2 term has other effects. It leads to elastic scattering of S with nuclei via Higgs exchange: $SN \rightarrow SN$. Direct detection experiments look for this process. In addition, if the S is sufficiently light – its mass is $M_S = \sqrt{\mu_S^2 + \frac{1}{2}\lambda_{hS}v_0^2}$ – the invisible decay of the Higgs, $h \rightarrow SS$, is possible. Finally, this term can also generate $SS \rightarrow \gamma\gamma$, a process that is relevant for indirect detection. It is therefore possible in principle that the SSDMM can account for all DM observations without the addition of any additional NP.

In 2017, a global fit of the SSDMM was performed, taking into account the measurements of the relic density, direct and indirect detection, and the invisible Higgs width [13]. (Other analyses of the SSDMM can be found in Refs. [54–57].) It was found that the value of λ_{hS} required to satisfy the relic density constraint implies a DM scattering rate on nuclei that exceeds the Xenon1T limits when $M_S \lesssim 500$ –700 GeV, except in some small (fine-tuned) regions of parameter space where $M_S \simeq 60$ GeV. And while the model is still viable for large values of M_S , for $M_S \gtrsim 5$ TeV, the required value of λ_{hS} becomes large, approaching the nonperturbative regime.

Note that Ref. [13] uses the 2017 direct detection constraints of the Xenon1T Collaboration [58] in its analysis of the SSDMM. These constraints have been improved recently (2021) by the PandaX-4T Collaboration [59]. While we do not perform a complete analysis of the SSDMM in this paper, in the next section we do show how these more-stringent direct detection constraints affect this model.

3 Effect on DM Observables

The most direct consequence of an $S^2 U_{1\mu}^\dagger U_1^\mu$ coupling is the generation of the tree-level annihilation process $SS \rightarrow U_1 \bar{U}_1$. It is well known that the process of DM annihilation takes place mostly at very small relative momentum, so that this process essentially does not occur for $M_S < M_{U_1} = 1.8$ TeV. In examining the effects of the $S^2 U_{1\mu}^\dagger U_1^\mu$ coupling on the various DM observables, it is therefore useful to consider separately heavy DM ($M_S \gtrsim M_{U_1} = 1.8$ TeV) and light DM ($M_S \lesssim M_{U_1} = 1.8$ TeV). In our analysis of the U_1 contributions to DM processes, we also include the Higgs-portal contributions.

Our DM analysis is performed using two different programs (to provide cross-checks): MadDM [60] and micrOMEGAs [61, 62]. The results for heavy and light DM presented below use MadDM and micrOMEGAs, respectively (unless otherwise indicated).

3.1 Heavy DM ($M_S \gtrsim M_{U_1} = 1.8$ TeV)

3.1.1 Relic Density

We begin by considering $M_S \gtrsim M_{U_1} = 1.8$ TeV. For this heavy DM, the lowest-order contribution of the U_1 portal to the relic density, namely $SS \rightarrow U_1 \bar{U}_1$, is possible.

As pointed out above, the $S^2 U_{1\mu}^\dagger U_1^\mu$ coupling will generate at one loop a $C_5^g S^2 G_{\mu\nu}^a G^{a\mu\nu}$ term [Eq. (10)] and an $SS\bar{f}f$ coupling [Eq. (13)]. These will lead to contribution to the relic density from the annihilations $SS \rightarrow gg$ and $SS \rightarrow f\bar{f}$. However, because they are essentially loop-level processes, they are negligible compared to $SS \rightarrow U_1 \bar{U}_1$.

DM annihilation takes place via both the Higgs and U_1 portals, whose couplings are respectively λ_{hS} and $\lambda_{U_1 S}$. To calculate the constraints from the relic density, we use MadDM [60]. We fix $M_{U_1} = 1.8$ TeV and take $\lambda_{U_1 S} = 0$ (pure Higgs portal), 0.04, 0.07 and 0.10. For each value of $\lambda_{U_1 S}$, we compute the value of λ_{hS} required to reproduce the relic density $\Omega h^2 = 0.1198 \pm 0.0012$ [9] to within $\pm 3\sigma$.

The results are shown in Fig. 3. We note the following:

- For $\lambda_{U_1 S} = 0$ (pure Higgs portal), the relic density can be reproduced for all values of M_S in the range $1 \text{ TeV} \leq M_S \leq 10 \text{ TeV}$. However, for $M_S \gtrsim 5$ TeV, the required value of the coupling λ_{hS} becomes large, approaching nonperturbative values.
- The addition of a nonzero $\lambda_{U_1 S}$ opens up the U_1 portal, so that the Higgs portal does not have to reproduce the relic density by itself. As a result, the required value of λ_{hS} is decreased. The size of the effect of the U_1 portal depends on the value of $\lambda_{U_1 S}$.

- Consider $\lambda_{U_1 S} = 0.10$. For $M_S \simeq 2$ TeV, the required value of λ_{hS} is smaller than for the case of a pure Higgs portal. As M_S increases, the rate for DM annihilation into $U_1 \bar{U}_1$ also increases, until at $M_S \simeq 4.5$ TeV, the Higgs portal is not even required ($\lambda_{hS} = 0$). But in this case, for even larger values of M_S , the annihilation rate into $U_1 \bar{U}_1$ is too large, so that the relic density is always below the measured value.
- One sees this same type of behaviour for smaller values of $\lambda_{U_1 S}$. For $\lambda_{U_1 S} = 0.07$, the maximal value of M_S is $\simeq 6$ TeV, while for $\lambda_{U_1 S} = 0.04$ it is between 10 and 11 TeV.
- Similarly, for each value of M_S , there is a value of $\lambda_{U_1 S}$ above which the relic density is too low. For example, for $M_S = 3$ TeV, $\lambda_{U_1 S} < 0.17$ is required.
- In the presence of the U_1 portal, the required value of λ_{hS} for $M_S \gtrsim 5$ TeV remains small and clearly perturbative, provided $\lambda_{U_1 S}$ is large enough, in contrast to the case of the pure Higgs portal.

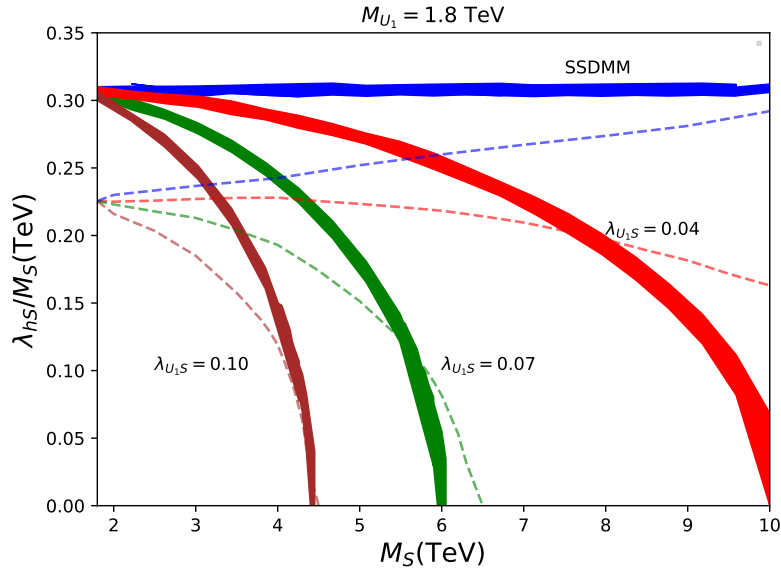


Figure 3: Value of $\lambda_{hS}/M_S(\text{TeV})$ required to reproduce the relic density in the SSDMM (blue) and in the modified SSDMM with $\lambda_{U_1 S} = 0.10$ (brown), 0.07 (green) and 0.04 (red), for $M_{U_1} = 1.8$ TeV. all as a function of M_S . Dashed lines indicate the future limits from indirect detection searches by CTA [63].

3.1.2 Indirect Detection

DM annihilation in galaxies also provides a method for indirect detection using various final states. Here we consider final states that contain photons. There are two different categories of such final states. First, there is the loop-induced process $SS \rightarrow \gamma\gamma$, which gives rise to a characteristic monoenergetic photon line at an energy of M_S . Second, the photons can be emitted from other final-state particles. Taking into account DM annihilation into all final states, this results in a continuous photon spectrum.

Photons from $SS \rightarrow \gamma\gamma$ were searched for by the H.E.S.S. Collaboration in observations from the inner Galactic halo [64]. However, the limits placed on the cross section are several orders of magnitude larger than what is predicted in our model. This is because, for heavy DM, $\lambda_{U_1 S}$ is much smaller than unity, leading to a significant suppression of this loop-induced process. H.E.S.S. also measured the continuous photon spectrum, placing constraints on the DM annihilation cross-section $\langle\sigma v\rangle \approx 10^{-24} \text{ cm}^3/\text{s}$ [65]. This is two orders of magnitude above the typical thermal cross-section of $\mathcal{O}(10^{-26} \text{ cm}^3/\text{s})$ found in our model.

More useful limits on DM annihilation will be obtained by the Cherenkov Telescope Array (CTA), which measures the continuous photon spectrum at higher energies [63], and is therefore relevant for TeV-scale DM.

Using micrOMEGAs.5.2, we compute the continuous photon spectrum for heavy DM annihilation into all final states. This value is then compared with the one that can be probed by CTA in the Galactic Center using the projections given in Ref. [63] and assuming an Einasto DM profile. To do this comparison, we use the likelihood tables provided in Ref. [66]. When $\lambda_{U_1 S} = 0$, the dominant SM final states are WW , ZZ and hh . In this case, we find that CTA will be able to probe the full region of the parameter space that leads to the correct relic density. This corresponds roughly to $\lambda_{hS} \simeq 0.25M_S$, and will rule out the SSDMM for heavy DM if no signal is observed.

As $\lambda_{U_1 S}$ increases such that the $SS \rightarrow U_1 \bar{U}_1$ contribution becomes more important, smaller values of λ_{hS} can be probed. Nevertheless, for each value of $\lambda_{U_1 S}$ shown in Fig. 3, when the DM mass exceeds a certain value, the relic-density-favoured region cannot be probed (e.g., for $\lambda_{U_1 S} = 0.10$, this value is $\simeq 4.5 \text{ TeV}$). In Sec. 3.1.1, we pointed out that, for each value of $\lambda_{U_1 S} > 0$, there is a value of M_S beyond which the DM annihilation channel into $U_1 \bar{U}_1$ becomes too efficient, and the relic density condition can never be satisfied. Similarly, there is a value of M_S for which DM annihilation in the galaxy is totally dominated by the U_1 final state and the CTA reach is independent of λ_{hS} . For example, for $\lambda_{U_1 S} = 0.10$ (0.07), this value is $\simeq 4.5 \text{ TeV}$ ($\simeq 6.5 \text{ TeV}$). Hence we conclude that, for $\lambda_{U_1 S} = 0.10$, the model can be completely probed by CTA, while for smaller values of $\lambda_{U_1 S}$, larger values of M_S are beyond the reach of CTA.

Note that when DM annihilates primarily into $U_1 \bar{U}_1$, the limit extracted from indirect detection shows little dependence on the U_1 couplings to fermions. For example, variations of $\pm 20\%$ in the couplings of Eq. (12) change the indirect detection

bounds by less than 1%.

3.1.3 Direct Detection

In Sec. 3.1.1, we saw that the addition of the U_1 portal has the effect of reducing the required value of λ_{hS} . But this has a downside as well. λ_{hS} is also the coefficient of the $v_0 h S^2$ term in Eq. (14), which leads to processes observable in direct detection experiments. Thus, a smaller value of λ_{hS} implies a decreased direct detection signal. In principle, this could be compensated for by direct detection signals using the U_1 LQ. Unfortunately, at tree level, there are no such signals. As a result, the addition of the U_1 portal has the effect of reducing the direct detection signal.

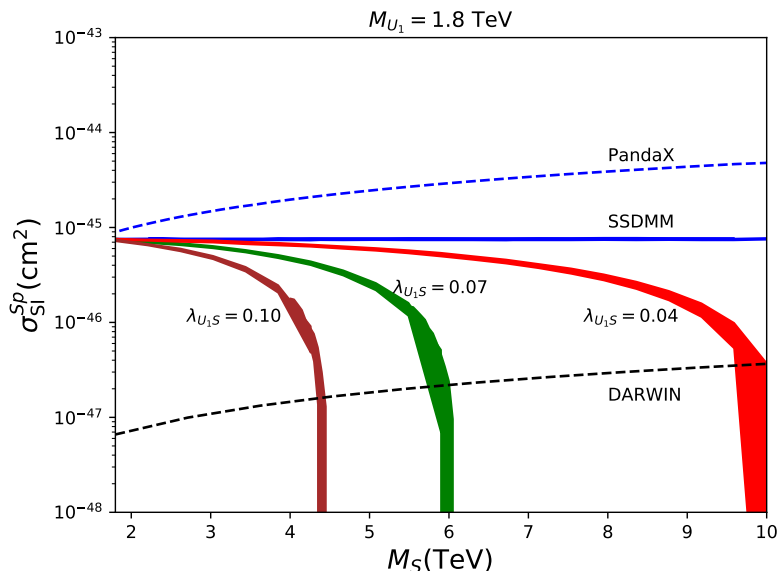


Figure 4: Predicted spin-independent cross section σ_{SI}^{Sp} in the SSDMM (blue) and in the modified SSDMM with $\lambda_{U_1 S} = 0.10$ (brown), 0.07 (green) and 0.04 (red), for $M_{U_1} = 1.8$ TeV. all as a function of M_S . The dashed lines are the present upper limit on the cross section from the PandaX-4T Collaboration [59] (blue) and the future reach of the DARWIN Collaboration [68] (black).

This is illustrated in Fig. 4, where we present the results for the spin-independent cross section for DM scattering off protons, σ_{SI}^{Sp} . If only the Higgs portal is available ($\lambda_{U_1 S} = 0$), the SSDMM yields a cross section $\sigma_{\text{SI}}^{Sp} \simeq 10^{-45}$ cm². If the U_1 portal is also open ($\lambda_{U_1 S} \neq 0$), this cross section decreases. The size of the decrease depends on how much λ_{hS} is reduced, which itself depends on the values of $\lambda_{U_1 S}$ and M_S , following the pattern of Fig. 3.

Note that there is also a contribution to $Sp \rightarrow Sp$ scattering due to the one-loop $SSgg$ coupling [Eq. (10)]. However, for heavy DM, this contribution is negligible

compared to that of the Higgs. (In the next subsection, we will see that this is not the case for light DM.)

At the present time, the upper limit on σ_{SI}^{Sp} from the PandaX-4T Collaboration is between 10^{-45} cm² and 10^{-44} cm², for $1 \text{ TeV} \leq M_S \leq 10 \text{ TeV}$ [59]. As can be seen from Fig. 4, this is still larger than the values predicted for the cross section in the SSDMM and the modified SSDMM, which includes the U_1 LQ. In the future, XENONnT [67] and DARWIN [68] will improve these constraints by almost two orders of magnitude. If no signal is observed, this will rule out the SSDMM. However, the modified SSDMM will still be viable for certain values of $\lambda_{U_1 S}$ and M_S .

3.2 Light DM ($M_S < M_{U_1} = 1.8 \text{ TeV}$)

For DM of mass $M_S < 1.8 \text{ TeV}$, annihilation via $SS \rightarrow U_1 \bar{U}_1$ is not possible. Instead, one must rely on the SSDMM. However, as shown in Ref. [13], this is problematic. For some values of M_S in this mass range, the value of the SSh coupling λ_{hS} required to reproduce the relic density via $SS \rightarrow h \rightarrow \text{SM particles}$ is in tension with the constraints from direct detection.

The one-loop $SSgg$ coupling generated via a virtual U_1 has the potential to help. First, it provides another annihilation channel, $SS \rightarrow gg$, so that the required value of λ_{hS} can be reduced. Second, it also contributes to the process $Sp \rightarrow Sp$ used for direct detection. It is possible that this contribution interferes destructively with that of the SSDMM, leading to weaker constraints on λ_{hS} from direct detection.

In addition, there is the possibility that one of the final-state LQs in $SS \rightarrow U_1 \bar{U}_1$ is virtual, leading to the three-body annihilation $SS \rightarrow U_1 \bar{q} \ell$. This could be important for $M_S > M_{U_1}/2$. To perform this calculation, we use the preferred couplings of the U_1 to $\bar{q} \ell$ given in Eq. (12). We include the contribution of the three-body annihilation channels in micrOMEGAs.5.2 as follows. We use the feature of micrOMEGAs that allows one to substitute a new annihilation cross section in the relic density calculation. We compute the cross-sections for all relevant three-body processes (namely $U_1 \tau b$, $U_1 \nu_\tau t$, $U_1 \tau s$, $U_1 \nu_\tau c$). From this we subtract $SS \rightarrow U_1 \bar{U}_1$ to avoid double counting when M_S is near M_{U_1} and the $U_1 \bar{U}_1$ can be produced on shell. This is then added to the two-body processes.

The consequence of all of these effects for the SSDMM is illustrated in Fig. 5. Here we compute the value of $\lambda_{hS}/M_S(\text{TeV})$ required to reproduce the relic density (within $\pm 3\sigma$) as a function of M_S . We overlay the constraints⁶ from the Xenon1T Collaboration [58] (2017) and the PandaX-4T Collaboration [59] (2021) due to their upper limit on the spin-independent cross section σ_{SI}^{Sp} .

⁶In order to compute σ_{SI}^{Sp} , we use the default values of micrOMEGAs for the coefficients of the quark content in the nucleon [51]. However, the $SSgg$ operator is ignored when computing the direct interaction rate. To simulate the effect of this operator, we introduce a new heavy quark and a new heavy scalar mediator (H_S) in the model, see Ref. [61]. The mediator couples only to the heavy quark and to DM as $\mathcal{L} = -m_Q \bar{Q} Q H_S + x S S H_S$, where $x = 21/16 \lambda_{U_1 S} M_{H_S}^2 / M_{U_1}^2$.

For the case of $\lambda_{U_1 S} = 0$ (pure Higgs portal), we see that, using the 2017 direct detection constraints from the Xenon1T Collaboration [58], there is a solution only for $M_S \gtrsim 950$ GeV. This explicitly demonstrates the problems for the SSDMM that were found in Ref. [13]⁷. But when the 2021 direct detection constraints from the PandaX-4T Collaboration [59] are used, one sees that these problems are worse: now, the SSDMM is viable only for $M_S \gtrsim 1.6$ TeV.

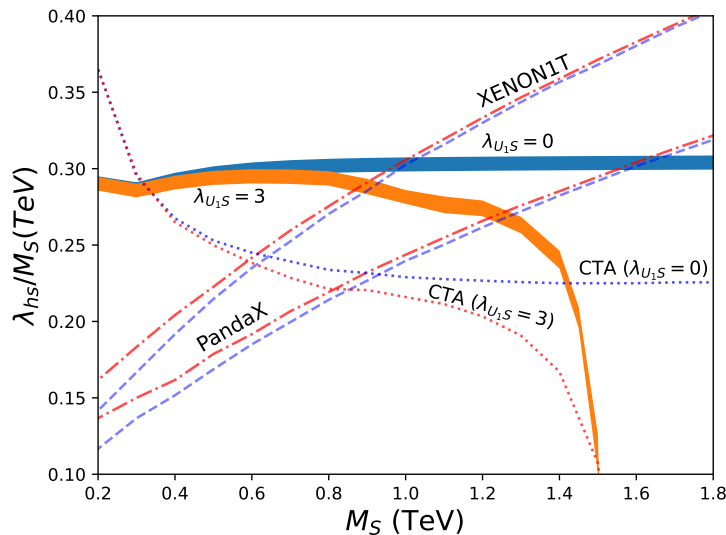


Figure 5: Values of $\lambda_{hS}/M_S(\text{TeV})$ required to reproduce the relic density (within $\pm 3\sigma$) as a function of M_S , for $\lambda_{U_1 S} = 0$ (blue band) and $\lambda_{U_1 S} = 3.0$ (orange band). Dashed lines show present constraints from the upper limit on the spin-independent cross section σ_{SI}^{Sp} [58] for the SSDMM (blue) and the SSDMM + U_1 (orange). Dotted lines indicate the future limits from indirect detection searches by CTA [63].

As expected, the situation improves when one adds the U_1 portal term $S^2 U_{1\mu}^\dagger U_1^\mu$. To be specific, with a (large) value of $\lambda_{hS} = 3.0$, the minimum value of M_S for which an explanation of the relic density can be found is reduced from $\simeq 1.6$ TeV to $\simeq 1.3$ TeV. There are several reasons for this. First, there are additional annihilation channels. $SS \rightarrow gg$ is possible for all values of M_S . And for $M_S > M_{U_1}/2$, the three-body annihilation $SS \rightarrow U_1 \bar{q} \ell$ opens up: the required value of $\lambda_{hS}/M_S(\text{TeV})$ begins to diminish at $M_S \simeq 1$ TeV, and falls precipitously at $M_S \simeq 1.65$ TeV. Second,

⁷Note that this restriction on M_S is not exactly the same as that found in Ref. [13]. This is because the analyses are not the same – we are simply taking into account constraints from the relic density and direct detection, while Ref. [13] performs a more complete global analysis. Still, the point is that the SSDMM had difficulties reproducing the data even in 2017.

the destructive interference of the $SSgg$ and Higgs contributions to $Sp \rightarrow Sp$ plays a (smaller) role.

We therefore conclude that, for light DM, the addition of the U_1 LQ does somewhat improve the outlook for the SSDMM (though not to the extent of allowing an explanation of the DM observables for $M_S = O(100)$ GeV).

As for indirect detection, the present bounds on $\sigma(SS \rightarrow \gamma\gamma)$ [64, 69] are several orders of magnitude larger than the prediction of our model. Even for $\lambda_{U_1 S} = 3$, which leads to the maximal effect, we obtain $v\sigma_{\gamma\gamma} = 5.5 \times 10^{-31} \text{ cm}^3/\text{s}$ for $M_S = 400$ GeV, while the bounds from FermiLAT (H.E.S.S.) are 4 (2.8) $\times 10^{-28} \text{ cm}^3/\text{s}$, assuming the Einasto profile. Similarly, for $M_S = 1000$ GeV, we predict $v\sigma_{\gamma\gamma} = 9.7 \times 10^{-30} \text{ cm}^3/\text{s}$, while the bound from H.E.S.S. is $3.5 \times 10^{-28} \text{ cm}^3/\text{s}$. From measurements of the continuous photon spectrum, FermiLAT can probe the thermal cross section only for DM masses around 100 GeV [70]. However, future measurements of the continuous photon spectrum from DM annihilation by CTA in the Galactic Center will be able to rule out the SSDMM and place stringent constraints on the modified SSDMM with $\lambda_{U_1 S} \neq 0$, as can be seen in Fig. 5.

Finally, an $S^2 U_{1\mu}^\dagger U_1^\mu$ coupling will also lead to the LHC scattering process $pp \rightarrow \ell^+ \ell^- SS$ via the t -channel exchange of a U_1 LQ. Here the SS would of course be “observed” as missing energy. We have computed the cross section for this process for $M_S = 100$ GeV. We find that, because the U_1 LQ is so heavy, and because it couples mainly to third-generation quarks [see Eq. (12)], the cross section is tiny: for $\lambda_{U_1 S} = O(1)$, $\sigma(pp \rightarrow \ell^+ \ell^- SS) = O(10^{-6})$ pb, which is unobservable.

4 Conclusions

At present, there are several B -decay observables whose measured values exhibit discrepancies with the predictions of the SM. These decays are mediated by $b \rightarrow s\mu^+\mu^-$ or $b \rightarrow c\tau^-\bar{\nu}$ transitions. It is possible to find NP models that explain both types of B anomalies. When all constraints are taken into account, only one model survives. It involves the addition of the U_1 LQ, a vector particle of charge $2/3$ that is an $SU(2)_L$ singlet and has a mass $M_{U_1} \gtrsim 1.8$ TeV.

Another observation that is unexplained by the SM is DM. A particularly simple scenario to explain the observed relic density is the scalar singlet dark matter model (SSDMM). We update the constraints on the SSDMM, taking into account the 2021 direct detection constraints from the PandaX-4T Collaboration. We find that this model is now viable only for $M_S \gtrsim 1.6$ TeV. Furthermore, for $M_S = O(\text{TeV})$, the required value of λ_{hS} enters the nonperturbative regime.

In an attempt to improve the prospects for the SSDMM, we add the U_1 LQ and assume a $\lambda_{U_1 S} S^2 U_{1\mu}^\dagger U_1^\mu$ coupling term. For heavy DM ($M_S \gtrsim M_{U_1}$), such a coupling leads to DM annihilation via $SS \rightarrow U_1 \bar{U}_1$. This coupling will also lead to $SSgg$ and $SS\gamma\gamma$ couplings at one loop. Although naively divergent, these loop diagrams can be computed by analogy to the SM hgg or $h\gamma\gamma$ couplings, under the assumption

that the U_1 is a gauge boson of a group broken at the TeV scale. The $SSgg$ and $SS\gamma\gamma$ couplings provide additional annihilation channels for light DM ($M_S < M_{U_1}$), and lead to signals of direct and indirect detection.

For heavy DM, the addition of the $SS \rightarrow U_1\bar{U}_1$ annihilation channel does indeed reduce the required value of λ_{hS} to below the nonperturbative level. The downside of this is that the direct detection signal is also reduced. Still, future direct detection experiments will be able to place constraints that will rule out the SSDMM, but the modified SSDMM will still be viable for certain values of λ_{U_1S} and M_S . And future indirect detection measurements will be able to place stringent constraints on the modified SSDMM.

For light DM, the $SSgg$ coupling provides another annihilation channel, and yields a contribution to direct detection that can interfere destructively with that of the SSDMM. And for $M_S > M_{U_1}/2$, one can have $SS \rightarrow U_1\bar{q}\ell$. The net effect of the U_1 LQ depends on the value of λ_{U_1S} . For $\lambda_{U_1S} = 3$, we find that the minimum value of M_S for which the DM data can be explained is reduced from $\simeq 1.6$ TeV to $\simeq 1.3$ TeV. As was the case with heavy DM, future indirect detection measurements will be able to place stringent constraints on this model.

Acknowledgments: We thank Diego Guadagnoli and M eril Reboud for discussions about related topics. This work was partially funded by the program ‘‘Aide aux  tudiants et d veloppement international de la R gion Auvergne Rhone-Alpes,’’ project number 1900811602-40889, by RFBR and CNRS, project number 20-52-15005 (GB, AP), and by NSERC of Canada (JK, DL). JK is financially supported by a postdoctoral research fellowship of the Alexander von Humboldt Foundation.

References

- [1] D. London and J. Matias, ‘‘ B Flavour Anomalies: 2021 Theoretical Status Report,’’ doi:10.1146/annurev-nucl-102020-090209 [arXiv:2110.13270 [hep-ph]].
- [2] M. Alguer , B. Capdevila, S. Descotes-Genon, J. Matias and M. Novoa-Brunet, ‘‘ $b \rightarrow s\ell\ell$ global fits after Moriond 2021 results,’’ [arXiv:2104.08921 [hep-ph]].
- [3] M. Blanke, A. Crivellin, T. Kitahara, M. Moscati, U. Nierste and I. Nišandžić, ‘‘Addendum to ‘‘Impact of polarization observables and $B_c \rightarrow \tau\nu$ on new physics explanations of the $b \rightarrow c\tau\nu$ anomaly’’,’’ doi:10.1103/PhysRevD.100.035035 [arXiv:1905.08253 [hep-ph]].
- [4] B. Bhattacharya, A. Datta, D. London and S. Shivashankara, ‘‘Simultaneous Explanation of the R_K and $R(D^{(*)})$ Puzzles,’’ Phys. Lett. B **742**, 370 (2015) doi:10.1016/j.physletb.2015.02.011 [arXiv:1412.7164 [hep-ph]].

- [5] B. Bhattacharya, A. Datta, J. P. Guévin, D. London and R. Watanabe, “Simultaneous Explanation of the R_K and $R_{D^{(*)}}$ Puzzles: a Model Analysis,” JHEP **1701**, 015 (2017) doi:10.1007/JHEP01(2017)015 [arXiv:1609.09078 [hep-ph]].
- [6] D. Buttazzo, A. Greljo, G. Isidori and D. Marzocca, “ B -physics anomalies: a guide to combined explanations,” JHEP **1711**, 044 (2017) doi:10.1007/JHEP11(2017)044 [arXiv:1706.07808 [hep-ph]].
- [7] J. Kumar, D. London and R. Watanabe, “Combined Explanations of the $b \rightarrow s\mu^+\mu^-$ and $b \rightarrow c\tau^-\bar{\nu}$ Anomalies: a General Model Analysis,” Phys. Rev. D **99**, no. 1, 015007 (2019) doi:10.1103/PhysRevD.99.015007 [arXiv:1806.07403 [hep-ph]].
- [8] A. Crivellin, D. Müller and T. Ota, “Simultaneous explanation of $R(D^{(*)})$ and $b \rightarrow s\mu^+\mu^-$: the last scalar leptoquarks standing,” JHEP **09**, 040 (2017) doi:10.1007/JHEP09(2017)040 [arXiv:1703.09226 [hep-ph]].
- [9] N. Aghanim *et al.* [Planck], “Planck 2018 results. VI. Cosmological parameters,” Astron. Astrophys. **641**, A6 (2020) [erratum: Astron. Astrophys. **652**, C4 (2021)] doi:10.1051/0004-6361/201833910 [arXiv:1807.06209 [astro-ph.CO]].
- [10] V. Silveira and A. Zee, “SCALAR PHANTOMS,” Phys. Lett. B **161** (1985), 136-140 doi:10.1016/0370-2693(85)90624-0
- [11] J. McDonald, “Gauge singlet scalars as cold dark matter,” Phys. Rev. D **50** (1994), 3637-3649 doi:10.1103/PhysRevD.50.3637 [arXiv:hep-ph/0702143 [hep-ph]].
- [12] C. P. Burgess, M. Pospelov and T. ter Veldhuis, “The Minimal model of non-baryonic dark matter: A Singlet scalar,” Nucl. Phys. B **619** (2001), 709-728 doi:10.1016/S0550-3213(01)00513-2 [arXiv:hep-ph/0011335 [hep-ph]].
- [13] P. Athron *et al.* [GAMBIT], “Status of the scalar singlet dark matter model,” Eur. Phys. J. C **77**, no.8, 568 (2017) doi:10.1140/epjc/s10052-017-5113-1 [arXiv:1705.07931 [hep-ph]].
- [14] D. Aristizabal Sierra, F. Staub and A. Vicente, “Shedding light on the $b \rightarrow s$ anomalies with a dark sector,” Phys. Rev. D **92**, no.1, 015001 (2015) doi:10.1103/PhysRevD.92.015001 [arXiv:1503.06077 [hep-ph]].
- [15] G. Bélanger, C. Delaunay and S. Westhoff, “A Dark Matter Relic From Muon Anomalies,” Phys. Rev. D **92**, 055021 (2015) doi:10.1103/PhysRevD.92.055021 [arXiv:1507.06660 [hep-ph]].
- [16] A. Celis, W. Z. Feng and M. Vollmann, “Dirac dark matter and $b \rightarrow s\ell^+\ell^-$ with U(1) gauge symmetry,” Phys. Rev. D **95**, no.3, 035018 (2017) doi:10.1103/PhysRevD.95.035018 [arXiv:1608.03894 [hep-ph]].

- [17] W. Altmannshofer, S. Gori, S. Profumo and F. S. Queiroz, “Explaining dark matter and B decay anomalies with an $L_\mu - L_\tau$ model,” JHEP **12**, 106 (2016) doi:10.1007/JHEP12(2016)106 [arXiv:1609.04026 [hep-ph]].
- [18] P. Ko, T. Nomura and H. Okada, “A flavor dependent gauge symmetry, Predictive radiative seesaw and LHCb anomalies,” Phys. Lett. B **772**, 547-552 (2017) doi:10.1016/j.physletb.2017.07.021 [arXiv:1701.05788 [hep-ph]].
- [19] P. Ko, T. Nomura and H. Okada, “Explaining $B \rightarrow K^{(*)}\ell^+\ell^-$ anomaly by radiatively induced coupling in $U(1)_{\mu-\tau}$ gauge symmetry,” Phys. Rev. D **95**, no.11, 111701 (2017) doi:10.1103/PhysRevD.95.111701 [arXiv:1702.02699 [hep-ph]].
- [20] J. M. Cline, J. M. Cornell, D. London and R. Watanabe, “Hidden sector explanation of B -decay and cosmic ray anomalies,” Phys. Rev. D **95**, no.9, 095015 (2017) doi:10.1103/PhysRevD.95.095015 [arXiv:1702.00395 [hep-ph]].
- [21] A. Falkowski, S. F. King, E. Perdomo and M. Pierre, “Flavourful Z' portal for vector-like neutrino Dark Matter and $R_{K^{(*)}}$,” JHEP **08**, 061 (2018) doi:10.1007/JHEP08(2018)061 [arXiv:1803.04430 [hep-ph]].
- [22] G. Arcadi, T. Hugle and F. S. Queiroz, “The Dark $L_\mu - L_\tau$ Rises via Kinetic Mixing,” Phys. Lett. B **784**, 151-158 (2018) doi:10.1016/j.physletb.2018.07.028 [arXiv:1803.05723 [hep-ph]].
- [23] P. T. P. Hutaauruk, T. Nomura, H. Okada and Y. Orikasa, “Dark matter and B -meson anomalies in a flavor dependent gauge symmetry,” Phys. Rev. D **99**, no.5, 055041 (2019) doi:10.1103/PhysRevD.99.055041 [arXiv:1901.03932 [hep-ph]].
- [24] A. Biswas and A. Shaw, “Reconciling dark matter, $R_{K^{(*)}}$ anomalies and $(g-2)_\mu$ in an $L_\mu - L_\tau$ scenario,” JHEP **05**, 165 (2019) doi:10.1007/JHEP05(2019)165 [arXiv:1903.08745 [hep-ph]].
- [25] Z. L. Han, R. Ding, S. J. Lin and B. Zhu, “Gauged $U(1)_{L_\mu-L_\tau}$ scotogenic model in light of $R_{K^{(*)}}$ anomaly and AMS-02 positron excess,” Eur. Phys. J. C **79**, no.12, 1007 (2019) doi:10.1140/epjc/s10052-019-7526-5 [arXiv:1908.07192 [hep-ph]].
- [26] D. Borah, L. Mukherjee and S. Nandi, “Low scale $U(1)_X$ gauge symmetry as an origin of dark matter, neutrino mass and flavour anomalies,” JHEP **12**, 052 (2020) doi:10.1007/JHEP12(2020)052 [arXiv:2007.13778 [hep-ph]].
- [27] J. M. Cline, “ B decay anomalies and dark matter from vectorlike confinement,” Phys. Rev. D **97**, no.1, 015013 (2018) doi:10.1103/PhysRevD.97.015013 [arXiv:1710.02140 [hep-ph]].

- [28] D. Guadagnoli, M. Reboud and P. Stangl, “The Dark Side of 4321,” JHEP **10**, 084 (2020) doi:10.1007/JHEP10(2020)084 [arXiv:2005.10117 [hep-ph]].
- [29] M. J. Baker, D. A. Farougy and S. Trifinopoulos, “Collider signatures of coannihilating dark matter in light of the B-physics anomalies,” JHEP **11**, 084 (2021) doi:10.1007/JHEP11(2021)084 [arXiv:2109.08689 [hep-ph]].
- [30] S. M. Choi, Y. J. Kang, H. M. Lee and T. G. Ro, “Lepto-Quark Portal Dark Matter,” JHEP **10**, 104 (2018) doi:10.1007/JHEP10(2018)104 [arXiv:1807.06547 [hep-ph]].
- [31] G. Bélanger, A. Bharucha, B. Fuks, A. Goudelis, J. Heisig, A. Jueid, A. Lessa, K. A. Mohan, G. Polesello and P. Pani, *et al.* “Leptoquark manoeuvres in the dark: a simultaneous solution of the dark matter problem and the $R_{D^{(*)}}$ anomalies,” JHEP **02**, 042 (2022) doi:10.1007/JHEP02(2022)042 [arXiv:2111.08027 [hep-ph]].
- [32] A. Crivellin, C. Greub, D. Müller and F. Saturnino, “Importance of Loop Effects in Explaining the Accumulated Evidence for New Physics in B Decays with a Vector Leptoquark,” Phys. Rev. Lett. **122**, no.1, 011805 (2019) doi:10.1103/PhysRevLett.122.011805 [arXiv:1807.02068 [hep-ph]].
- [33] N. Assad, B. Fornal and B. Grinstein, “Baryon Number and Lepton Universality Violation in Leptoquark and Diquark Models,” Phys. Lett. B **777**, 324-331 (2018) doi:10.1016/j.physletb.2017.12.042 [arXiv:1708.06350 [hep-ph]].
- [34] L. Di Luzio, A. Greljo and M. Nardecchia, “Gauge leptoquark as the origin of B -physics anomalies,” Phys. Rev. D **96**, no.11, 115011 (2017) doi:10.1103/PhysRevD.96.115011 [arXiv:1708.08450 [hep-ph]].
- [35] L. Calibbi, A. Crivellin and T. Li, “Model of vector leptoquarks in view of the B -physics anomalies,” Phys. Rev. D **98**, no.11, 115002 (2018) doi:10.1103/PhysRevD.98.115002 [arXiv:1709.00692 [hep-ph]].
- [36] M. Bordone, C. Cornella, J. Fuentes-Martin and G. Isidori, “A three-site gauge model for flavor hierarchies and flavor anomalies,” Phys. Lett. B **779**, 317-323 (2018) doi:10.1016/j.physletb.2018.02.011 [arXiv:1712.01368 [hep-ph]].
- [37] R. Barbieri and A. Tesi, “ B -decay anomalies in Pati-Salam $SU(4)$,” Eur. Phys. J. C **78**, no.3, 193 (2018) doi:10.1140/epjc/s10052-018-5680-9 [arXiv:1712.06844 [hep-ph]].
- [38] M. Blanke and A. Crivellin, “ B Meson Anomalies in a Pati-Salam Model within the Randall-Sundrum Background,” Phys. Rev. Lett. **121**, no.1, 011801 (2018) doi:10.1103/PhysRevLett.121.011801 [arXiv:1801.07256 [hep-ph]].

- [39] U. Aydemir, D. Minic, C. Sun and T. Takeuchi, “ B -decay anomalies and scalar leptoquarks in unified Pati-Salam models from noncommutative geometry,” JHEP **09**, 117 (2018) doi:10.1007/JHEP09(2018)117 [arXiv:1804.05844 [hep-ph]].
- [40] J. Heeck and D. Teresi, “Pati-Salam explanations of the B -meson anomalies,” JHEP **12**, 103 (2018) doi:10.1007/JHEP12(2018)103 [arXiv:1808.07492 [hep-ph]].
- [41] S. Balaji, R. Foot and M. A. Schmidt, “Chiral $SU(4)$ explanation of the $b \rightarrow s$ anomalies,” Phys. Rev. D **99**, no.1, 015029 (2019) doi:10.1103/PhysRevD.99.015029 [arXiv:1809.07562 [hep-ph]].
- [42] B. Fornal, S. A. Gadam and B. Grinstein, “Left-Right $SU(4)$ Vector Leptoquark Model for Flavor Anomalies,” Phys. Rev. D **99**, no.5, 055025 (2019) doi:10.1103/PhysRevD.99.055025 [arXiv:1812.01603 [hep-ph]].
- [43] S. Balaji and M. A. Schmidt, “Unified $SU(4)$ theory for the $R_{D^{(*)}}$ and $R_{K^{(*)}}$ anomalies,” Phys. Rev. D **101**, no.1, 015026 (2020) doi:10.1103/PhysRevD.101.015026 [arXiv:1911.08873 [hep-ph]].
- [44] S. Iguro, J. Kawamura, S. Okawa and Y. Omura, “TeV-scale vector leptoquark from Pati-Salam unification with vectorlike families,” Phys. Rev. D **104**, no.7, 075008 (2021) doi:10.1103/PhysRevD.104.075008 [arXiv:2103.11889 [hep-ph]].
- [45] A. Greljo and B. A. Stefanek, “Third family quark–lepton unification at the TeV scale,” Phys. Lett. B **782**, 131-138 (2018) doi:10.1016/j.physletb.2018.05.033 [arXiv:1802.04274 [hep-ph]].
- [46] C. Cornella, J. Fuentes-Martin and G. Isidori, “Revisiting the vector leptoquark explanation of the B -physics anomalies,” JHEP **1907**, 168 (2019) doi:10.1007/JHEP07(2019)168 [arXiv:1903.11517 [hep-ph]].
- [47] A. Angelescu, D. Bečirević, D. A. Faroughy, F. Jaffredo and O. Sumensari, “Single leptoquark solutions to the B-physics anomalies,” Phys. Rev. D **104**, no.5, 055017 (2021) doi:10.1103/PhysRevD.104.055017 [arXiv:2103.12504 [hep-ph]].
- [48] R. M. Godbole, G. Mendiratta and T. M. P. Tait, “A Simplified Model for Dark Matter Interacting Primarily with Gluons,” JHEP **08**, 064 (2015) doi:10.1007/JHEP08(2015)064 [arXiv:1506.01408 [hep-ph]].
- [49] C. Biggio, M. Bordone, L. Di Luzio and G. Ridolfi, “Massive vectors and loop observables: the $g - 2$ case,” JHEP **10**, 002 (2016) doi:10.1007/JHEP10(2016)002 [arXiv:1607.07621 [hep-ph]].

- [50] W. J. Marciano, C. Zhang and S. Willenbrock, “Higgs Decay to Two Photons,” *Phys. Rev. D* **85**, 013002 (2012) doi:10.1103/PhysRevD.85.013002 [arXiv:1109.5304 [hep-ph]].
- [51] G. Belanger, F. Boudjema, A. Pukhov and A. Semenov, “micrOMEGAs_3: A program for calculating dark matter observables,” *Comput. Phys. Commun.* **185**, 960-985 (2014) doi:10.1016/j.cpc.2013.10.016 [arXiv:1305.0237 [hep-ph]].
- [52] J. R. Ellis, M. K. Gaillard and D. V. Nanopoulos, “A Phenomenological Profile of the Higgs Boson,” *Nucl. Phys. B* **106**, 292 (1976) doi:10.1016/0550-3213(76)90382-5
- [53] M. Beltran, D. Hooper, E. W. Kolb and Z. C. Krusberg, “Deducing the nature of dark matter from direct and indirect detection experiments in the absence of collider signatures of new physics,” *Phys. Rev. D* **80**, 043509 (2009) doi:10.1103/PhysRevD.80.043509 [arXiv:0808.3384 [hep-ph]].
- [54] K. Cheung, Y. L. S. Tsai, P. Y. Tseng, T. C. Yuan and A. Zee, “Global Study of the Simplest Scalar Phantom Dark Matter Model,” *JCAP* **10**, 042 (2012) doi:10.1088/1475-7516/2012/10/042 [arXiv:1207.4930 [hep-ph]].
- [55] J. M. Cline, K. Kainulainen, P. Scott and C. Weniger, “Update on scalar singlet dark matter,” *Phys. Rev. D* **88**, 055025 (2013) [erratum: *Phys. Rev. D* **92**, no.3, 039906 (2015)] doi:10.1103/PhysRevD.88.055025 [arXiv:1306.4710 [hep-ph]].
- [56] A. Beniwal, F. Rajec, C. Savage, P. Scott, C. Weniger, M. White and A. G. Williams, “Combined analysis of effective Higgs portal dark matter models,” *Phys. Rev. D* **93**, no.11, 115016 (2016) doi:10.1103/PhysRevD.93.115016 [arXiv:1512.06458 [hep-ph]].
- [57] P. Athron, J. M. Cornell, F. Kahlhoefer, J. McKay, P. Scott and S. Wild, “Impact of vacuum stability, perturbativity and XENON1T on global fits of \mathbb{Z}_2 and \mathbb{Z}_3 scalar singlet dark matter,” *Eur. Phys. J. C* **78**, no.10, 830 (2018) doi:10.1140/epjc/s10052-018-6314-y [arXiv:1806.11281 [hep-ph]].
- [58] E. Aprile *et al.* [XENON], “First Dark Matter Search Results from the XENON1T Experiment,” *Phys. Rev. Lett.* **119**, no.18, 181301 (2017) doi:10.1103/PhysRevLett.119.181301 [arXiv:1705.06655 [astro-ph.CO]].
- [59] Y. Meng *et al.* [PandaX-4T], “Dark Matter Search Results from the PandaX-4T Commissioning Run,” *Phys. Rev. Lett.* **127**, no.26, 261802 (2021) doi:10.1103/PhysRevLett.127.261802 [arXiv:2107.13438 [hep-ex]].
- [60] F. Ambroggi, C. Arina, M. Backovic, J. Heisig, F. Maltoni, L. Mantani, O. Mattelaer and G. Mohlabeng, “MadDM v.3.0: a Comprehensive Tool for Dark Matter Studies,” *Phys. Dark Univ.* **24**, 100249 (2019) doi:10.1016/j.dark.2018.11.009 [arXiv:1804.00044 [hep-ph]].

- [61] G. Bélanger, F. Boudjema, A. Pukhov and A. Semenov, “Dark matter direct detection rate in a generic model with micrOMEGAs 2.2,” *Comput. Phys. Commun.* **180**, 747-767 (2009) doi:10.1016/j.cpc.2008.11.019 [arXiv:0803.2360 [hep-ph]].
- [62] G. Bélanger, F. Boudjema, A. Goudelis, A. Pukhov and B. Zaldivar, “micrOMEGAs5.0 : Freeze-in,” *Comput. Phys. Commun.* **231**, 173-186 (2018) doi:10.1016/j.cpc.2018.04.027 [arXiv:1801.03509 [hep-ph]].
- [63] A. Acharyya *et al.* [CTA], “Sensitivity of the Cherenkov Telescope Array to a dark matter signal from the Galactic centre,” *JCAP* **01**, 057 (2021) doi:10.1088/1475-7516/2021/01/057 [arXiv:2007.16129 [astro-ph.HE]].
- [64] H. Abdallah *et al.* [HESS], “Search for γ -Ray Line Signals from Dark Matter Annihilations in the Inner Galactic Halo from 10 Years of Observations with H.E.S.S.,” *Phys. Rev. Lett.* **120**, no.20, 201101 (2018) doi:10.1103/PhysRevLett.120.201101 [arXiv:1805.05741 [astro-ph.HE]].
- [65] L. Oakes *et al.* [Fermi-LAT, HAWC, H.E.S.S., MAGIC and VERITAS], “Combined Dark Matter searches towards dwarf spheroidal galaxies with *Fermi*-LAT, HAWC, HESS, MAGIC and VERITAS,” *PoS ICRC2019*, 012 (2021) doi:10.22323/1.358.0012 [arXiv:1909.06310 [astro-ph.HE]].
- [66] T. Bringmann, C. Eckner, A. Sokolenko, L. Yang and G. Zaharijas, “Likelihoods for the CTA sensitivity to a dark matter signal from the Galactic centre,” <https://zenodo.org/record/4022241#.Ype4cmjMJp0> .
- [67] E. Aprile *et al.* [XENON], “Physics reach of the XENON1T dark matter experiment,” *JCAP* **04**, 027 (2016) doi:10.1088/1475-7516/2016/04/027 [arXiv:1512.07501 [physics.ins-det]].
- [68] J. Aalbers *et al.* [DARWIN], “DARWIN: towards the ultimate dark matter detector,” *JCAP* **11**, 017 (2016) doi:10.1088/1475-7516/2016/11/017 [arXiv:1606.07001 [astro-ph.IM]].
- [69] M. Ackermann *et al.* [Fermi-LAT], “Updated search for spectral lines from Galactic dark matter interactions with pass 8 data from the Fermi Large Area Telescope,” *Phys. Rev. D* **91**, no.12, 122002 (2015) doi:10.1103/PhysRevD.91.122002 [arXiv:1506.00013 [astro-ph.HE]].
- [70] M. Ackermann *et al.* [Fermi-LAT], “Searching for Dark Matter Annihilation from Milky Way Dwarf Spheroidal Galaxies with Six Years of Fermi Large Area Telescope Data,” *Phys. Rev. Lett.* **115**, no.23, 231301 (2015) doi:10.1103/PhysRevLett.115.231301 [arXiv:1503.02641 [astro-ph.HE]].